Supporting Information

The Quest for Electrokinetic Control over Bulk Zeolite Synthesis: Trials, Effects and Challenges

Mostafa Torka Beydokhti[a]‡, *Gleb Ivanushkin*[a]‡, *Michiel Dusselier*[a]*

[a] Center for Sustainable Catalysis and Engineering (CSCE), KU Leuven, B-3001 Leuven, Belgium

‡ Equal contribution.

*Corresponding author: michiel.dusselier@kuleuven.be

Materials

CBV 720 (Zeolite Y, Zeolyst, Si/Al=15); CBV 300 (Zeolite Y, Zeolyst, Si/Al=2.5); Zeolite A4 (Union Carbide, Si/Al=1) Tetraethyl orthosilicate (TEOS, Acros Organics, 98 %); LUDOX AS-40 colloidal silica (Sigma-Aldrich, 40 wt. %); LUDOX HS-40 colloidal silica (Sigma-Aldrich, 40 wt.%); Sodium metasilicate anhydrous (Na_2SiO_3, Fisher Scientific, tech.); Tetramethylammonium hydroxide (TMAOH, Alfa Aesar, 25 wt. %); Tetramethylammonium chloride (Fisher Scientific, 98 %); Tetraethylammonium hydroxide (ZeoGen, 40 wt. %); Tetrapropylammonium hydroxide (TPAOH, Fisher Scientific, 25 wt. %); N,N,N-Trimethyl-1-adamantylammonium Hydroxide (TMAdamOH, ZeoGen, 25 wt. %); Aluminum isopropoxide (Sigma-Aldrich, ≥ 99%); Sodium aluminate ($AlH_4O_4.Na$, Sigma-Aldrich, Al_2O_3: 50-56%, Na_2O: 37-45%); Aluminum isopropoxide (Acros Organics, 98 %); Aluminum sulfate octadecahydrate ($Al_2(SO_4)_3.18H_2O$, Sigma-Aldrich, ≥ 98%); Aluminum-tri-sec-butoxide (Acros Organics, 97 %); Sodium hydroxide (NaOH, Sigma-Aldrich, ≥98%); Sodium chloride (NaCl, VWR, ≥99%); Potassium hydroxide (KOH, Sigma-Aldrich, 99.99%); Strontium hydroxide ($Sr(OH)_2$, Sigma-Aldrich, 94 wt. %); Cesium hydroxide monohydrate ($CsOH.H_2O$, Sigma-Aldrich, 99.5%); Hydrofluoric acid (HF, Sigma-Aldrich, 40 wt. % in water); Hydrochloric acid (HCl, Acros Organics, 37 wt. % in water); Nitric acid (HNO_3, Acros Organics, 65 wt. % in water]; Boric acid [H_3BO_3, Chem-Lab, ≥99.5%]; Aceton (CH_3COCH_3, VWR, ≥99%); Deionized water Mili-Q, 18.2 mΩ.

Table S1: Zeolite synthesis systems selected for EKC.

Entry	Framework	Chemical molar formula	Temp. (℃)	Time (h)	Ref.
1	EAB/FAU	1 Si:0.15 Al:0.53 $TMAOH$:0.57 $NaOH$:27 H_2O	80	24-72	1
2	FAU/LTA	1 Si:0.46 Al:$(1.12-x)$ $TMAOH$:x $NaOH$:56 H_2O x: 0-1.12	100	24-72	2
3	Low-silica CHA	1 Si:0.4 Al:4.08 KOH: 0.01 $Sr(OH)_2$:204 H_2O	100	6-120	3,4
4	FAU/LTA	1 Si:0.67 Al:2 $NaOH$:34 H_2O	65	168	5
5	EMT/FAU	1 Si:0.4 Al:8 $NaOH$:136 H_2O	30	24	6
6	NaA	1 Si:0.27 Al:2$TMAOH$: 0.07 $NaOH$:90 H_2O	60	168	7
7	Na-UZM-9	1 Si:0.125 Al:1 $TEAOH$:0.0625 $TMACl$: 0.0625 $NaCl$:34 H_2O	100	96	8
8	BPH	1 Si:0.16 Al:0.06 $CsOH$: 0.25 KOH: 1.61 $NaOH$: 11 H_2O	30	120	9
9	Embryonic CHA	1 Si:0.067 Al:0.3 $TMAdamOH$:14.5 H_2O	100	96	10
10	MFI	1 Si:0.36 $TPAOH$:20 H_2O	90	168	11

Preparation of synthesis mixtures

The synthesis recipes were adapted from references[1–11] listed in Table S1.

1- The final molar composition of the gel for EAB/FAU system according to ref.[1] was 1 Si:0.15 Al:0.53 $TMAOH$:0.57 $NaOH$:27 H_2O. First, solution A was prepared by dissolving sodium aluminate in half of the water DI together with sodium hydroxide. Solution B was prepared by mixing 40 wt.% LUDOX HS-40 colloidal silica in the remaining water together with 25 wt.% tetramethylammonium hydroxide. After 30 min stirring, solution A was added dropwise to solution B, which was kept in an ice bath under vigorous stirring. The final mixture formed a dense gel.

2- The final molar composition for the FAU/LTA system using OSDA according to ref.[2] was $1\,Si{:}0.46\,Al{:}(1.12-x)\,TMAOH{:}x\,NaOH{:}56\,H_2O$ where x was changed between 0 and 1.12. First, sodium hydroxide (if any) and 40 wt.% tetramethylammonium hydroxide were added to DI water. Then, under the stirring, aluminum isopropoxide was added to obtain a clear solution. To the previous solution, LUDOX AS-40 colloidal silica was added and the solution was left for aging for 72 h.

3- The low-silica CHA zeolite molar composition was $1\,Si{:}0.4\,Al{:}4.08\,KOH{:}\,0.01\,Sr(OH)_2{:}204\,H_2O$ according to ref.[3,4]. First, potassium hydroxide and strontium hydroxide were mixed in DI water until full dissolution. Then, aluminum sulfate octadecahydrate was added to the solution under mixing to result in a homogeneous solution. Finally, LUDOX AS-40 was added and the mixture was kept under stirring for 24 h of aging.

4- The FAU/LTA system without OSDA molar composition according to ref.[5] was $1\,Si{:}0.67\,Al{:}2\,NaOH{:}34\,H_2O$. First, sodium aluminate and sodium hydroxide were mixed in DI water under stirring to obtain a clear solution. Then, LUDOX AS-40 colloidal silica was added as the silica source and the solution was kept under stirring for 24 h before synthesis.

5- The EMT/FAU system molar composition according to ref.[6] was $1\,Si{:}0.4\,Al{:}8\,NaOH{:}136\,H_2O$. Sodium hydroxide and sodium aluminate were mixed in DI water. After obtaining a clear solution, sodium metasilicate anhydrous was added and kept under stirring for 10 min before synthesis.

6- The NaA zeolite synthesis mixture was prepared using molar composition of $1\,Si{:}0.27\,Al{:}2TMAOH{:}\,0.07\,NaOH{:}90\,H_2O$ according to ref.[7]. Sodium hydroxide, 40 wt.% tetramethylammonium hydroxide and aluminum isopropoxide were mixed in DI water. To the previous solution, TEOS was added and the solution was kept under stirring for TEOS hydrolysis completion.

7- The Na-UZM-9 zeolite mixture was prepared using molar composition $1\,Si{:}0.125\,Al{:}1\,TEAOH{:}0.0625\,TMACl{:}\,0.0625\,NaCl{:}34\,H_2O$ based on ref.[8]. First, solution A was prepared by mixing aluminum-tri-sec-butoxide in a solution of 40 wt.% Tetraethylammonium hydroxide in DI water. Solution A was kept under stirring for 2 h to result in a clear solution. To solution A, TEOS was added and left under stirring for another 2 h for TEOS hydrolysis and ethanol evaporation. Solution B was prepared by dissolving sodium chloride and tetramethylammonium chloride in DI water. Solution B was added to solution A under stirring to obtain a clear solution before synthesis.

8- The BPH zeolite solution was prepared based on ref.[9] using molar composition $1\,Si{:}0.16\,Al{:}0.06\,CsOH{:}\,0.25\,KOH{:}\,1.61\,NaOH{:}\,11\,H_2O$. Under high-speed stirring, sodium aluminate was dissolved in DI water and sodium hydroxide was added, followed by potassium hydroxide. After dissolution of potassium hydroxide, an aqueous solution of cesium hydroxide monohydrate was added. The solution was then kept for 2 h under stirring to obtain a clear solution. To this, LUDOX AS-40 colloidal silica was added dropwise and the mixture was left for 24 h of aging.

9- Embryonic CHA was synthesized using molar composition $1\,Si{:}0.067\,Al{:}0.3\,TMAdamOH{:}14.5\,H_2O$ adopted from ref.[10]. First, 25 wt.% N,N,N-Trimethyl-1-adamantylammonium Hydroxide was mixed in DI water. Then, CBV 720 was added as the silicon source. The solution was kept under stirring for 5 min to be homogenized.

10- Pure silica MFI zeolite mixture was prepared using molar composition $1\,Si{:}0.36\,TPAOH{:}20\,H_2O$ according to ref.[11]. TEOS and 25 wt.% tetrapropylammonium hydroxide were mixed in DI and the solution was kept under stirring for 24 h.

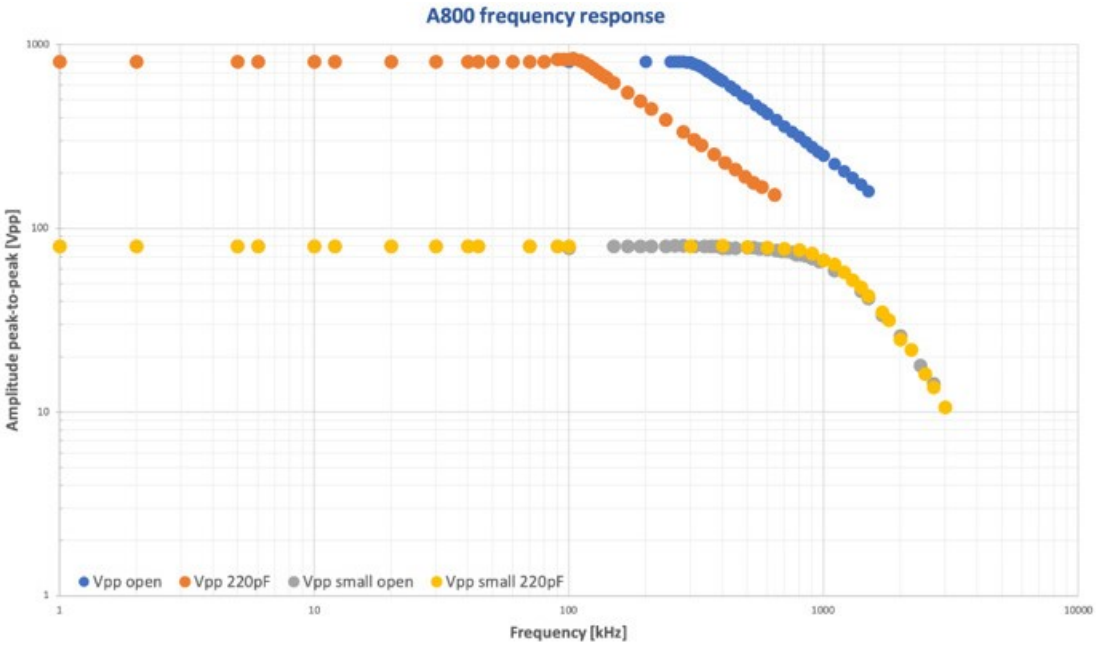

Figure S1. Full and small-signal frequency responses without load and with 220 pF capacitive load, respectively. Copied from ref. [12].

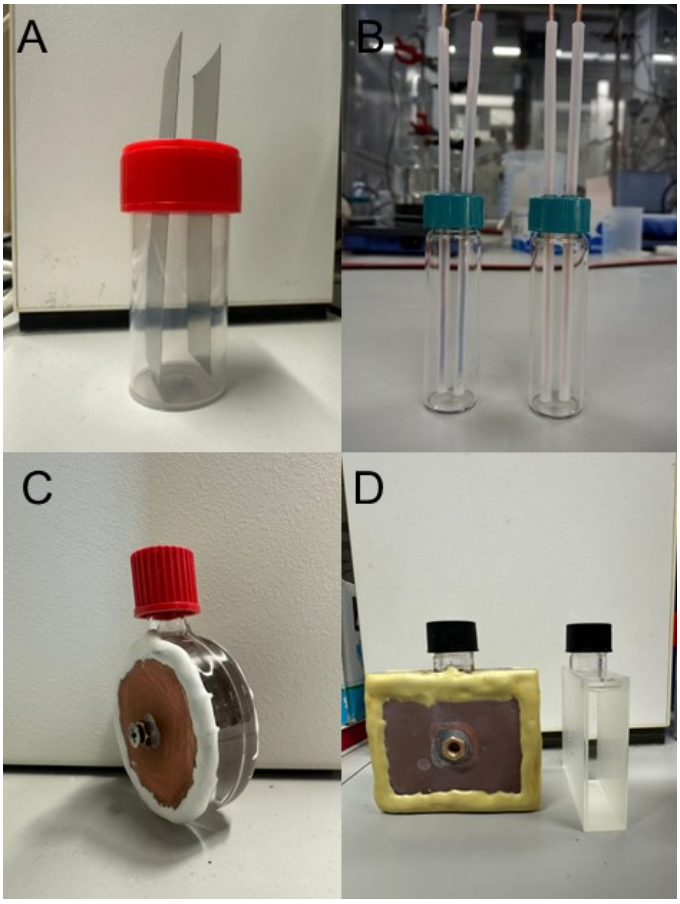

Figure S2. Reactors' images used for EKC: A) Internal plate electrodes in 30 ml polypropylene bottles (Type 1), B) PTFE-coated rod electrodes inside 7-ml glass vials (Type 2), C) Circular glass reactors with 1 and 1.5 cm electrode spacing (Type 3), D) Quartz cuvettes with plate electrodes (Type 4). The sealing and electrode fixing were done using glue.

Table S2. Characteristics of reactors shown in Figure S1 and corresponding EFs. C is the circular glass bottles that are used with two different electrode spacing, called C1 and C2.

Reactor			**Volume (ml)**	**$Area_{Electrode}$ (cm^2)**	**$Area_{Electrode}$/Volume (cm^2/ml)**	**Glass thickness (mm)**	**Electrode space (cm)**	**EF mode**	**EF strength (V/m)**
Type	**Label in Fig. S2**								
1	**A**		40	32	1.06	-	1	-	-
2	**B**		7	-	-	-	0.5	Nonuniform	-
3	**C**	**C1**	8	19.4	2.4	2.5	1	Uniform	$< 2 \times 10^6$
		C2	30	19.4	0.65	2.5	2	Uniform	$< 10^6$
4	D		20	20	1	1.125	1.25	Uniform	$< 1.04 \times 10^6$

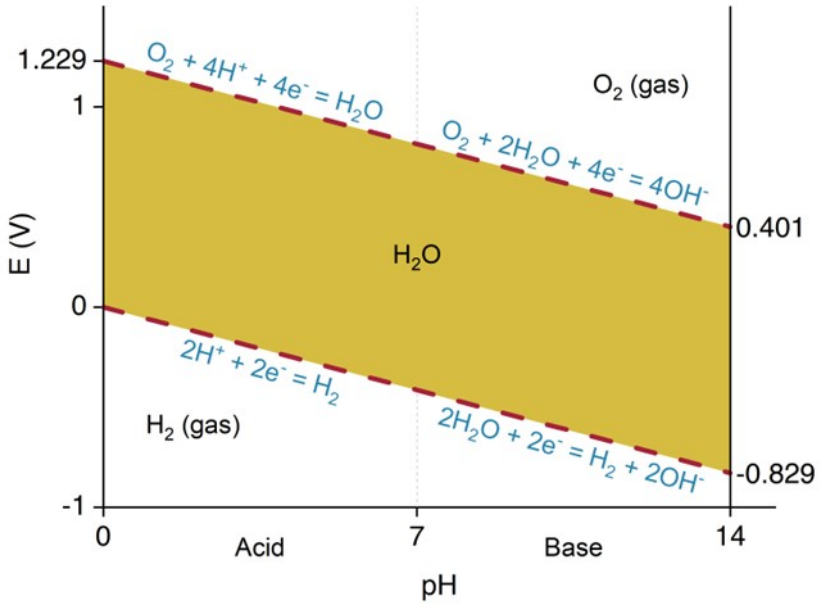

Figure S3. Pourbaix diagram for water, including equilibrium regions for water, oxygen, and hydrogen at standard temperature and pressure.

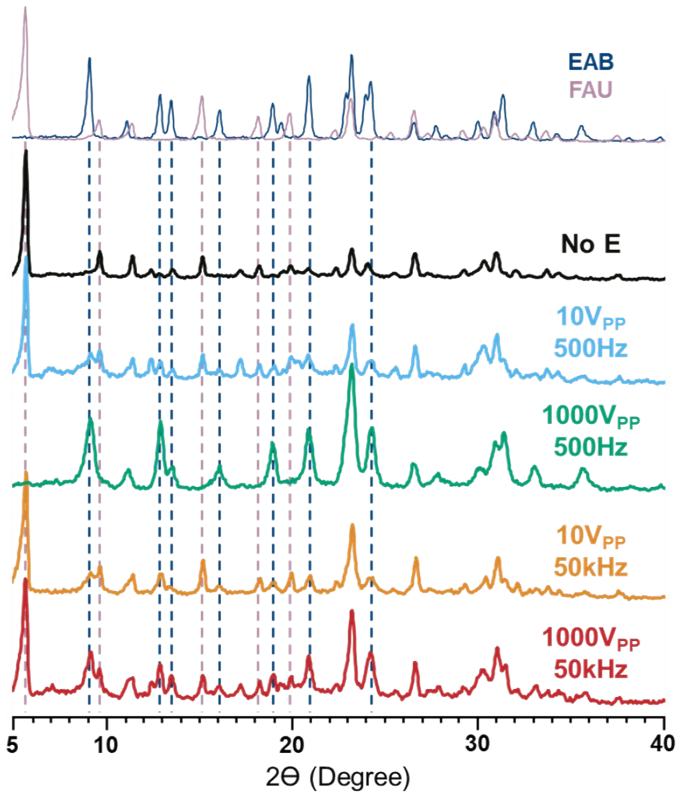

Figure S4. Selectivity of phase formation tested in the Type 1 reactor: **10** vs **1000V$_{PP}$** at **500** and **50kHz**. EAB and FAU model diffractogram simulations are found on the top. The FAU pattern was measured from CBV300 (Zeolyst) and EAB pattern was measured from a synthesized powder according to ref. [1].

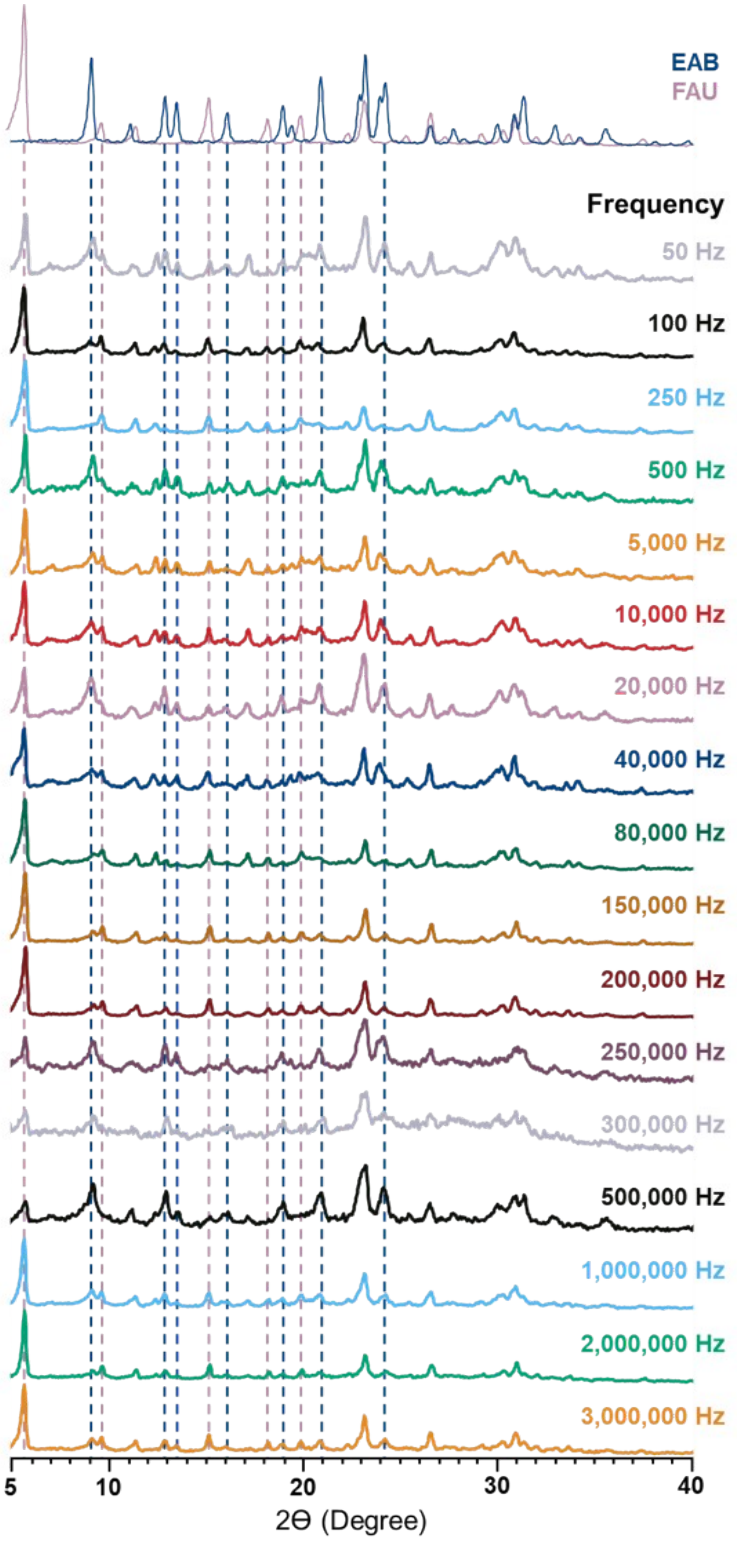

Figure S5. PXRD patterns of materials resulting from FAU/EAB competitive synthesis under applied internal EF: varied frequencies at **20V_{PP}** voltage. EAB and FAU model diffractogram simulations are found on the top. The FAU pattern was measured from CBV300 (Zeolyst) and EAB pattern was measured from a synthesized powder according to ref. [1].

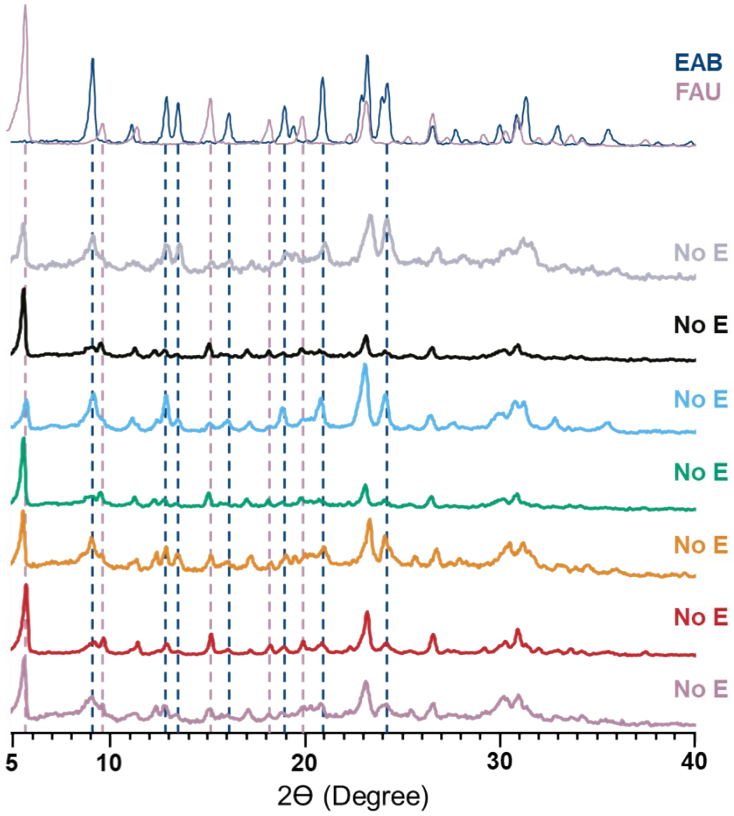

Figure S6. PXRD patterns of materials resulting from FAU/EAB competitive synthesis in silent conditions. EAB and FAU model diffractogram simulations are found on the top. The FAU pattern was measured from CBV300 (Zeolyst) and EAB pattern was measured from a synthesized powder according to ref. [1].

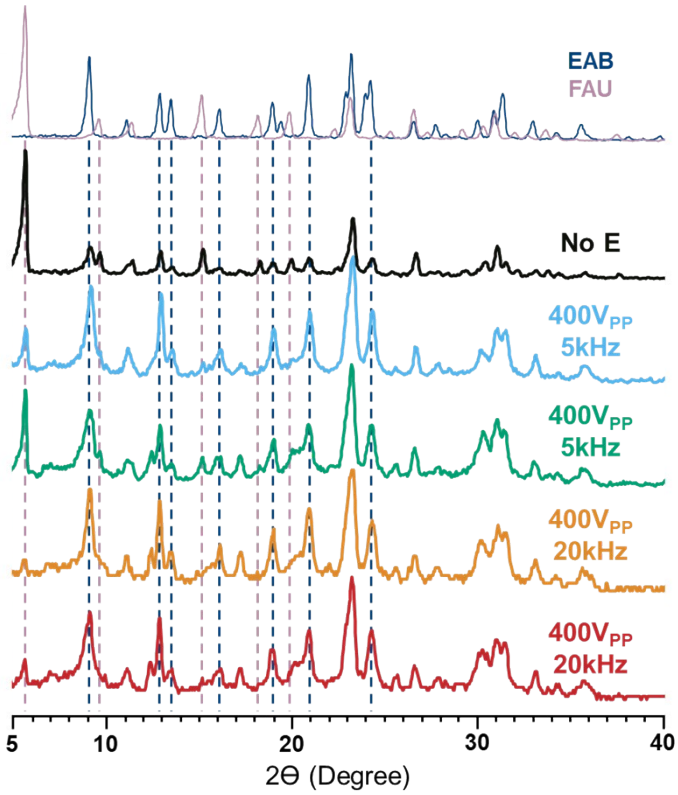

Figure S7. Reproducibility study: Selectivity of phase formation tested in the Type 1 reactor at **400V$_{PP}$** at **5** and **20kHz**. EAB and FAU model diffractogram simulations are found on the top. The FAU pattern was measured from CBV300 (Zeolyst) and EAB pattern was measured from a synthesized powder according to ref. [1].

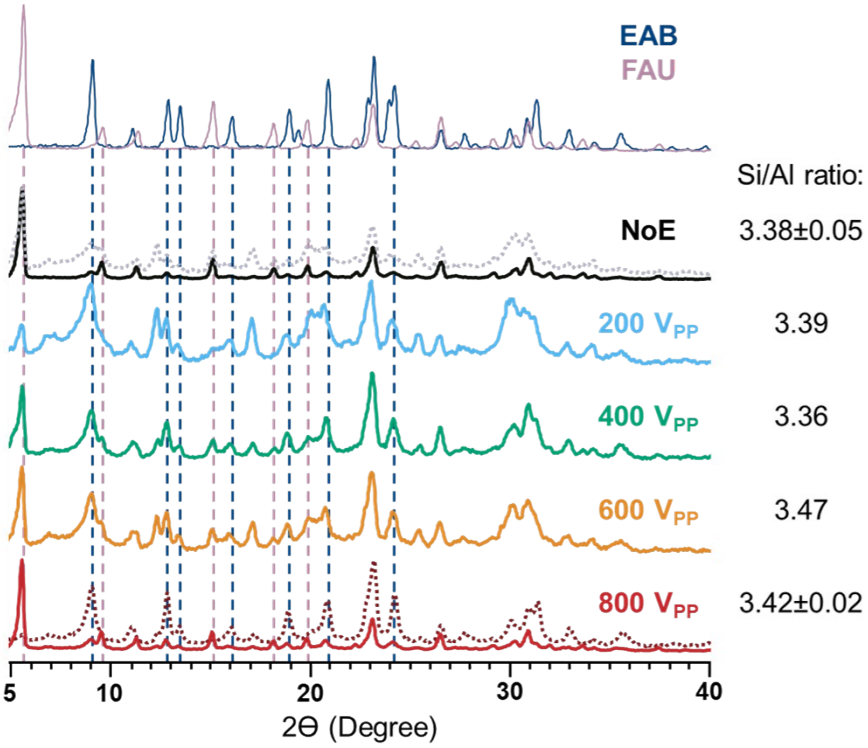

Figure S8. PXRD patterns of materials resulting from FAU/EAB competitive synthesis under applied internal EF: varied voltages at **787.6 Hz** frequency. The reference pattern of FAU zeolite belongs to CBV300, while the pure-phase EAB zeolite reference was successfully reproduced from the book of verified zeolite synthesis. Final bulk Si/Al ratio of zeolites was measured by ICP and listed in the right column, the error bar comes from two separate elemental analysis on different samples made in the same conditions.

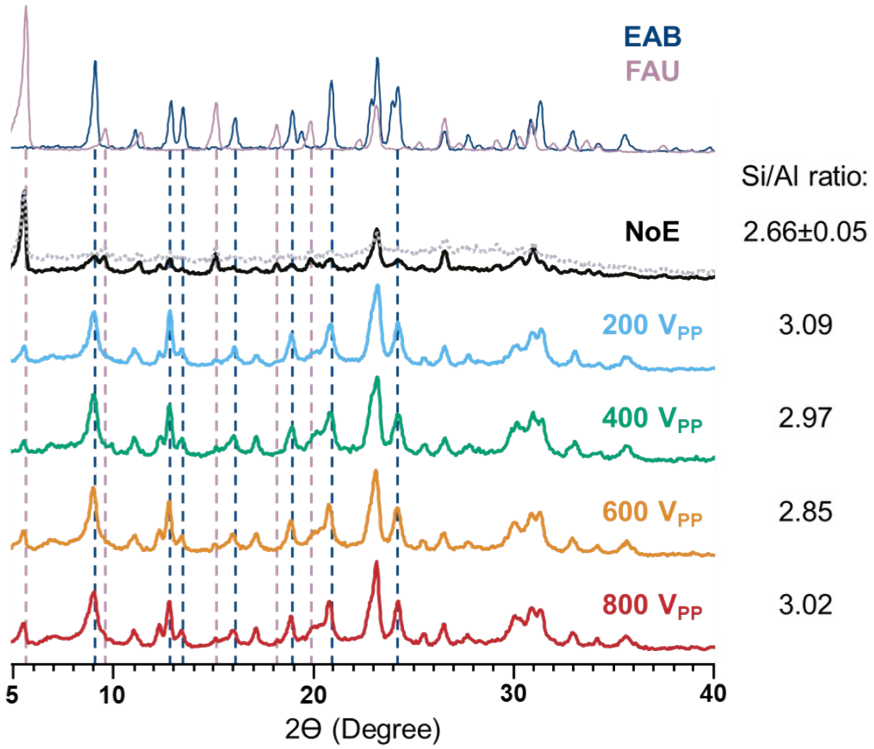

Figure S9. PXRD patterns of materials resulting from FAU/EAB competitive synthesis under applied internal EF: varied voltages at **5,000 Hz** (5kHz) frequency. Final bulk Si/Al ratio of zeolites was measured by ICP and listed in the right column, the error bar comes from two separate elemental analysis on different samples made in the same conditions.

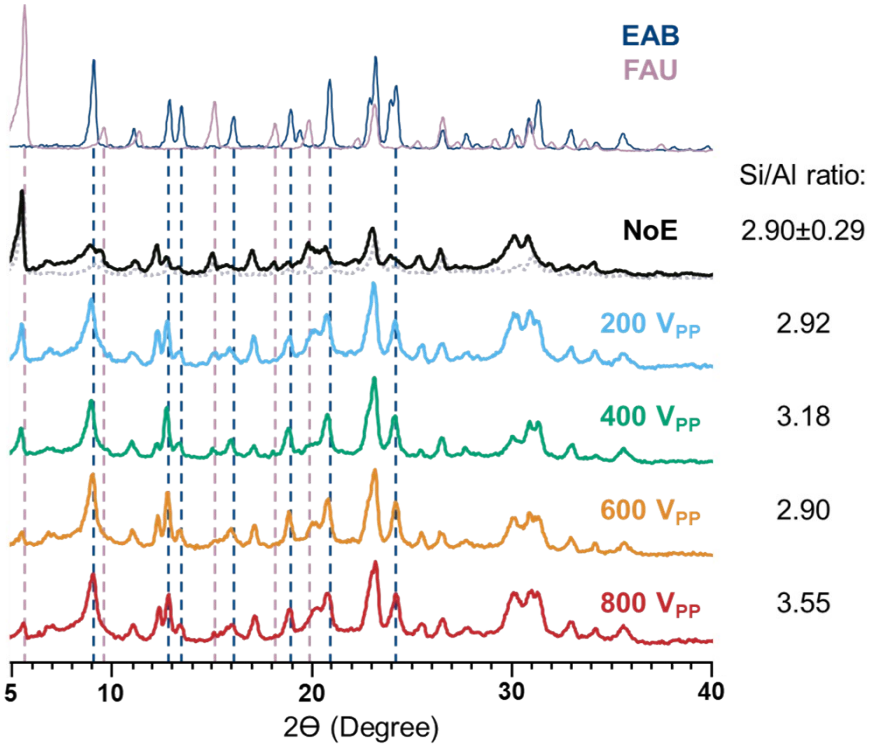

Figure S10. PXRD patterns of materials resulting from FAU/EAB competitive synthesis under applied internal EF: varied voltages at **40,000 Hz** (40kHz) frequency. Final bulk Si/Al ratio of zeolites was measured by ICP and listed in the right column, the error bar comes from two separate elemental analysis on different samples made in the same conditions.

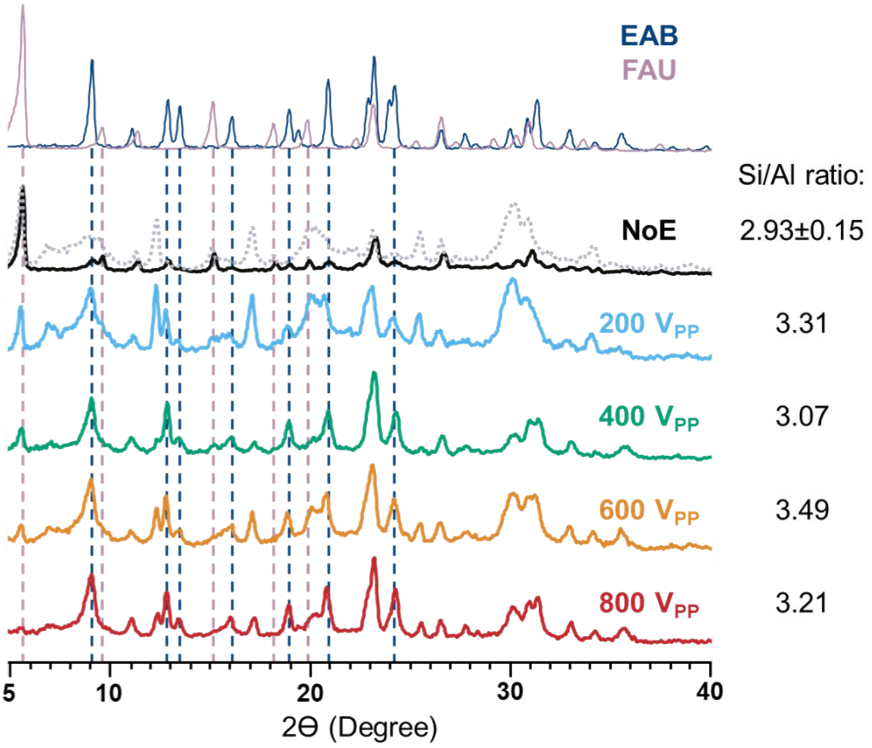

Figure S11. PXRD patterns of materials resulting from FAU/EAB competitive synthesis under applied internal EF: varied voltages at **50,000 Hz** (50kHz) frequency. Final bulk Si/Al ratio of zeolites was measured by ICP and listed in the right column, the error bar comes from two separate elemental analysis on different samples made in the same conditions.

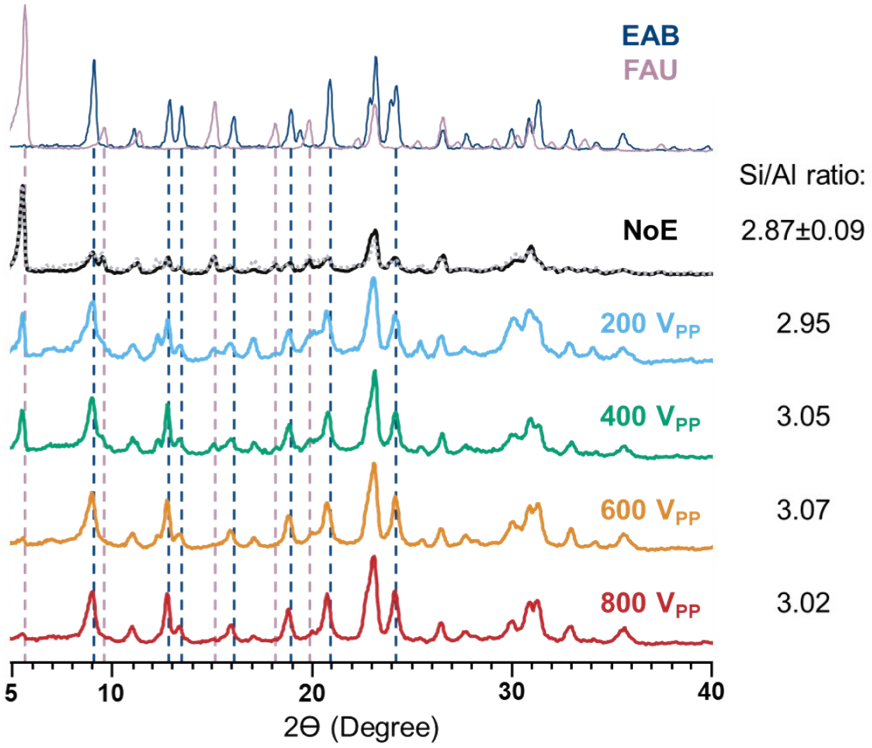

Figure S12. PXRD patterns of materials resulting from FAU/EAB competitive synthesis under applied internal EF: varied voltages at **100,000 Hz** (100kHz) frequency. Final bulk Si/Al ratio of zeolites was measured by ICP and listed in the right column, the error bar comes from two separate elemental analysis on different samples made in the same conditions.

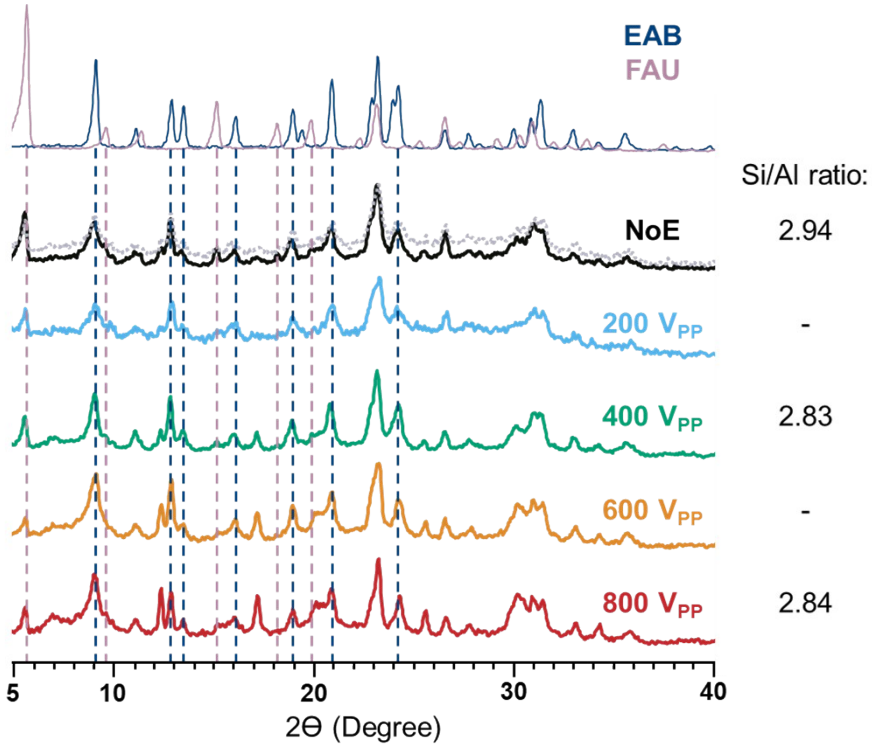

Figure S13. PXRD patterns of materials resulting from FAU/EAB competitive synthesis under applied internal EF: varied voltages at **1,000,000 Hz** (1MHz) frequency. Final bulk Si/Al ratio of zeolites was measured by ICP and listed in the right column, the error bar comes from two separate elemental analysis on different samples made in the same conditions.

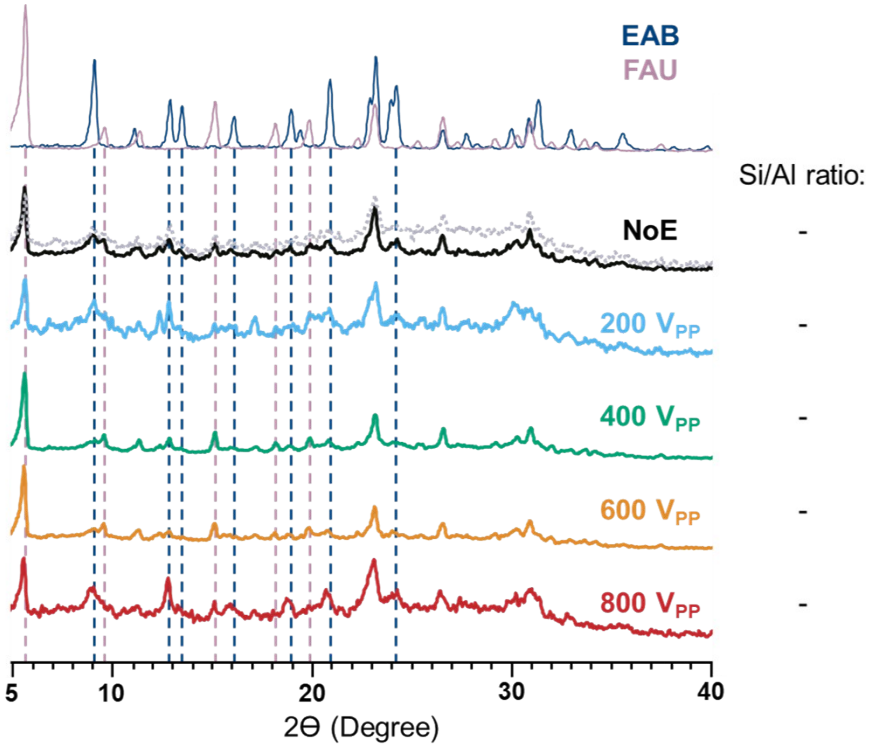

Figure S14. PXRD patterns of materials resulting from FAU/EAB competitive synthesis under applied internal EF: varied voltages at **30,000,000 Hz** (30MHz) frequency. Final bulk Si/Al ratio of zeolites was measured by ICP and listed in the right column, the error bar comes from two separate elemental analysis on different samples made in the same conditions.

EAB/FAU synthesis under DC EFs using Type 2 reactors:

According to the original work, using the synthesis gel (Si/Al 6.6, TMAOH, 80 °C, details in Table S1, entry 1), the expected product is pure-phase EAB[1]. However, we observed that minor variations in synthesis conditions could shift the phase selectivity toward FAU. Specifically, when stirring was applied inside the vials, replicating the original synthesis protocol, FAU formation was detected after 48 hours under an EF of 400 V_{PP} (no change in polarity, 1 μHz frequency). This phase was absent under batch conditions and in the absence of an EF (Absence of EF is specified as 0V, Figure S15). Interestingly, at an EF of 800 V_{PP}, the FAU phase was not present (Figure S15D). Under 400 V_{PP} EF without stirring, phase outcomes were inconsistent, and FAU was not reliably formed across experiments. Additionally, the absence of stirring in batch conditions also led to FAU formation. After 72 hours of crystallization, the Si/Al ratio of the zeolites was found to be identical for all, the batch, 0 V and 400 V_{PP} (Table S3). The DC EAB/FAU systems seemed inconclusive, perhaps due to the fact that initial gel in this system is dense and viscous, as evidenced by its tendency to adhere to the walls of the vials after synthesis (Figure S16). To reduce mass transfer limitations and enhance charge migration, we further focused on more dilute systems.

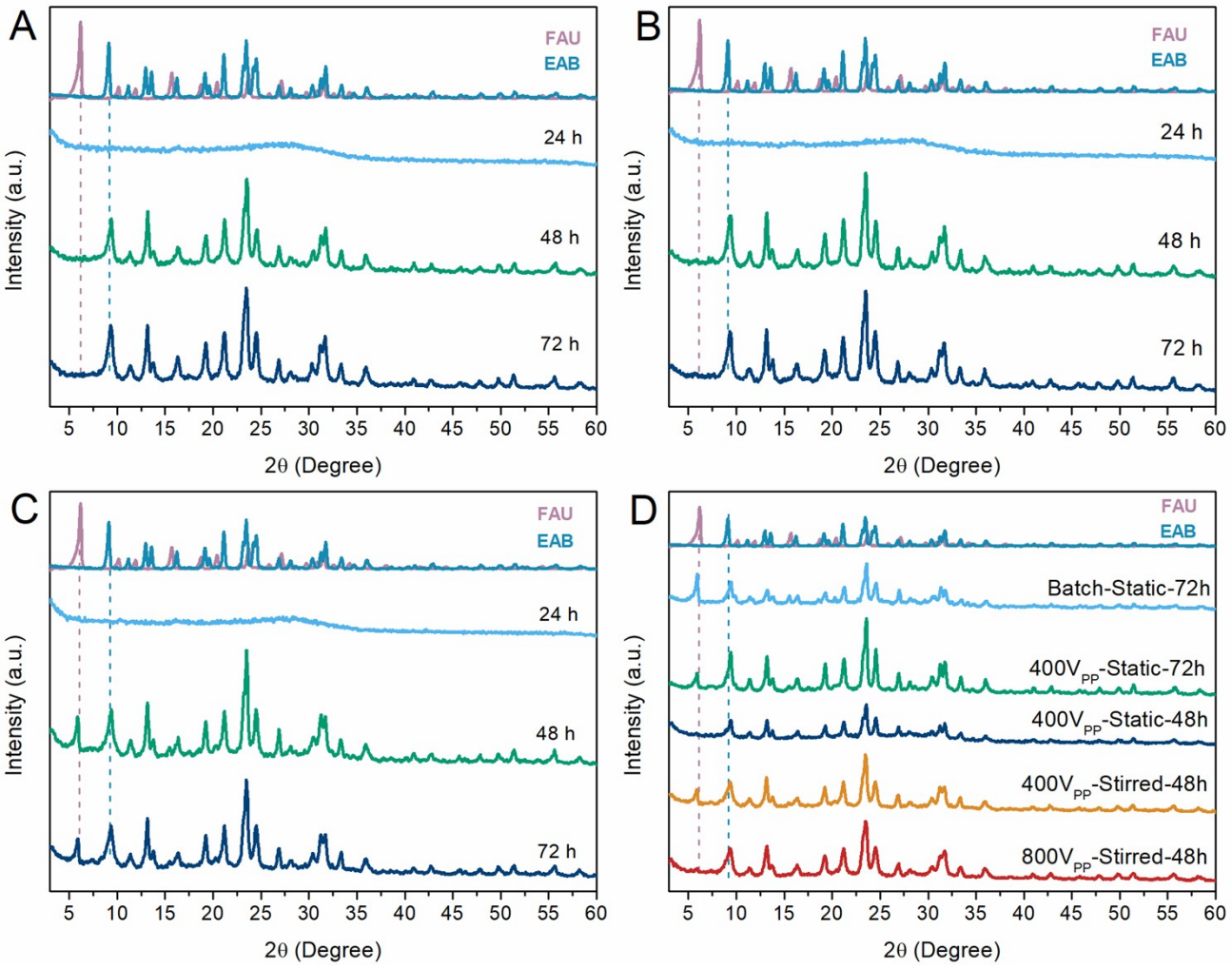

Figure S15. PXRD patterns of solid products at 24, 48 and 72 h for A) batch synthesis, B) Internal electrodes without EF (0V), C) under **400 V_{pp}** EF in presence of stirring (500 rpm) inside the reactors and D) Comparison of PXRD patterns of zeolites derived from batch and EKC synthesis with and without stirring. The FAU pattern was measured from CBV300 (Zeolyst) and EAB pattern was measured from a synthesized powder according to ref. [1].

Table S3. Si/Al ratio of zeolites taken after 72h synthesis of EAB/FAU system. The elemental compositions were obtained from ICP-EOS analysis.

Sample	**Si/Al molar ratio**
7ml vials	
Batch-Stirred-72h	2.4
0V-Stirred-72h	2.4
400 V_{pp}-Stirred-72h	2.3

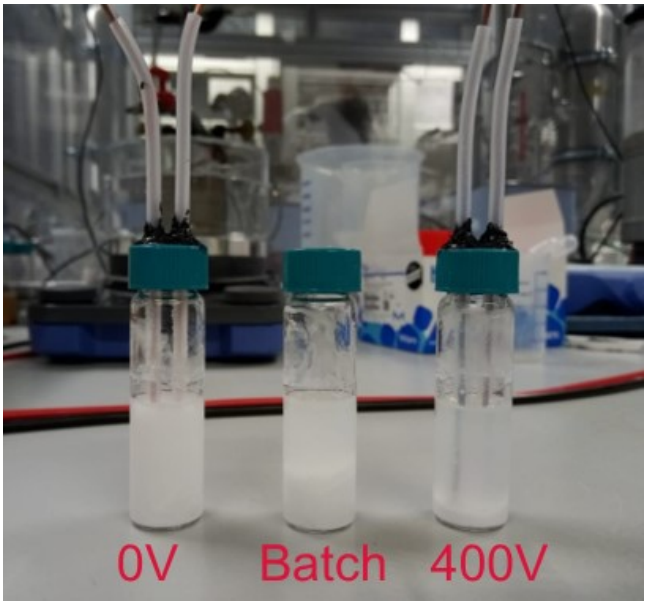

Figure S16. EAB/FAU synthetic mixture for batch, 0V and **400 V_{PP}** after 72 h heating at 80°C.

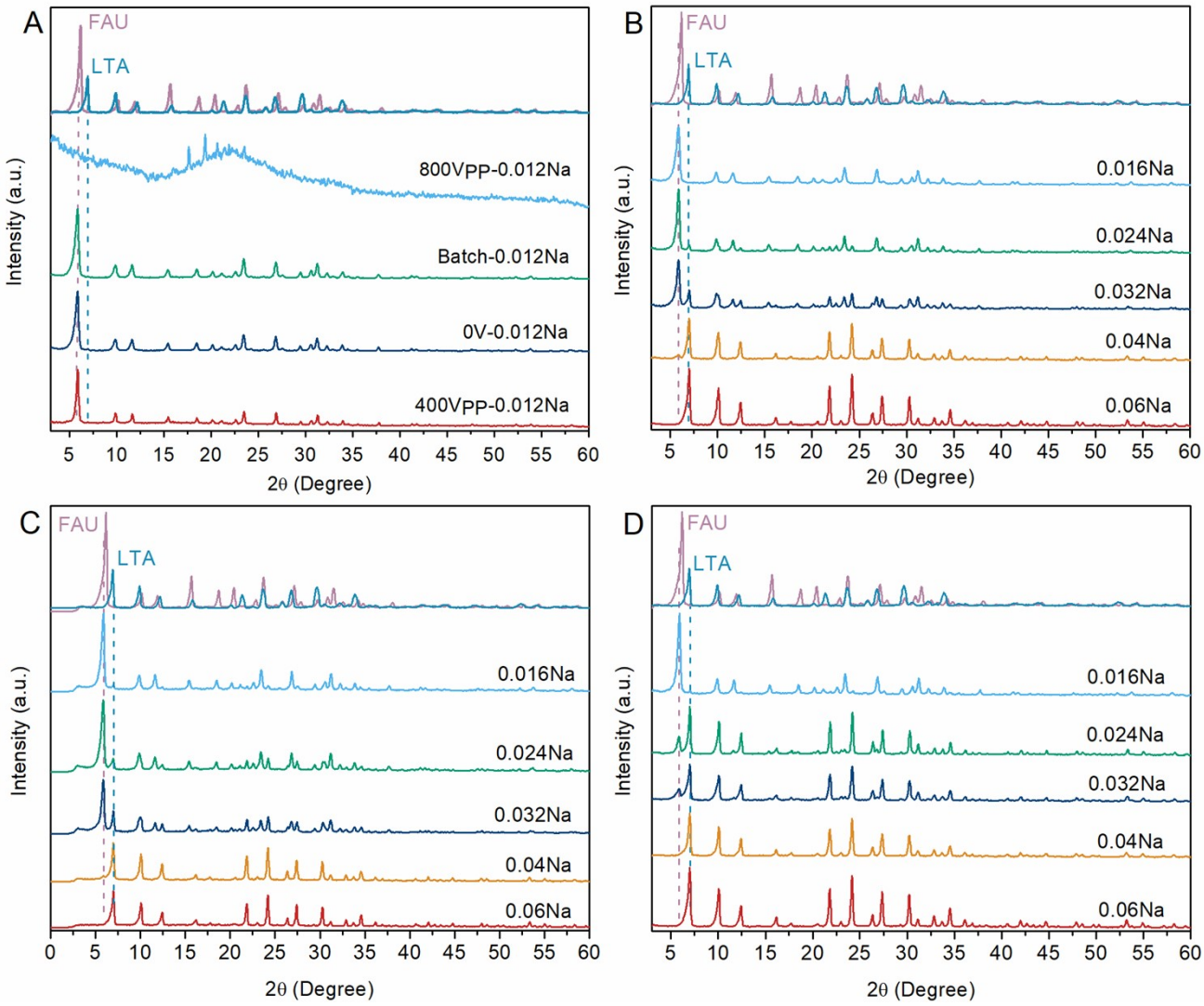

Figure S17. A) PXRD patterns of FAU/LTA synthesis without NaOH under **800 V_{PP}** and with NaOH/Si of 0.012 in Batch, 0V and under **400 V_{PP}**. PXRD patterns of samples obtained from FAU/LTA system at different NaOH concentrations for B) Batch, C) 0V and D) under EF of **400 V_{PP}**. The molar composition of the synthesis mixture is presented in Table S1. FAU and LTA reference patterns were measured from CBV300 and zeolite 4A.

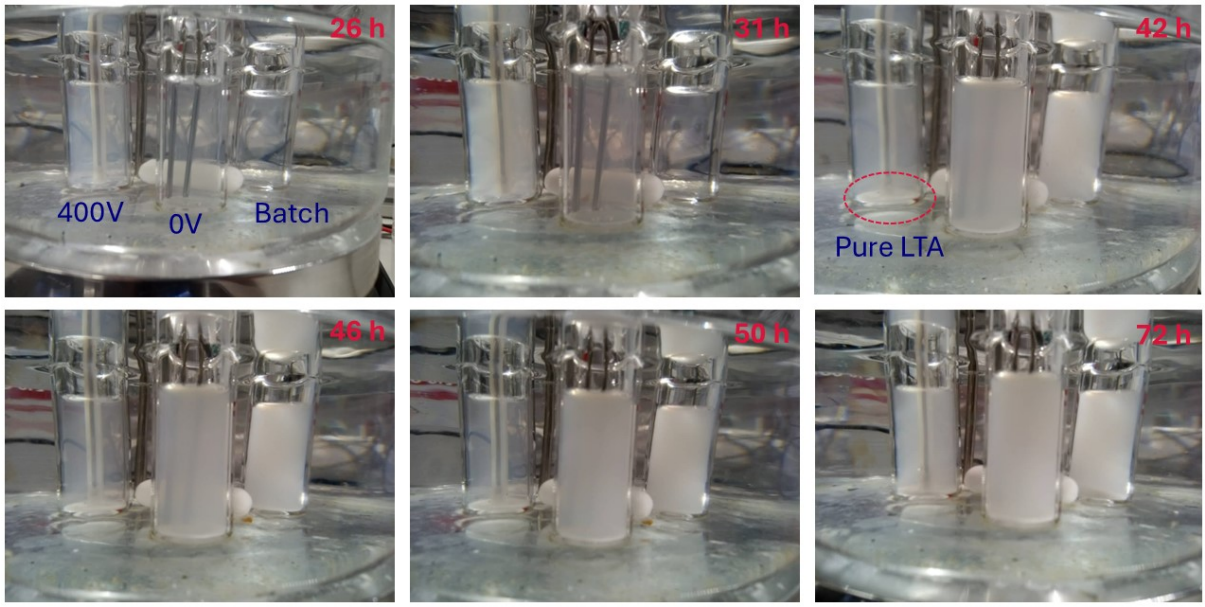

Figure S18. Photos of synthesis vials during the crystallization at different times for NaOH/Si of 0.024 in FAU/LTA system, Table S1, entry 2. Note: In this experiment, the 0V reactors include stainless steel rods instead of PTFE-coated wires.

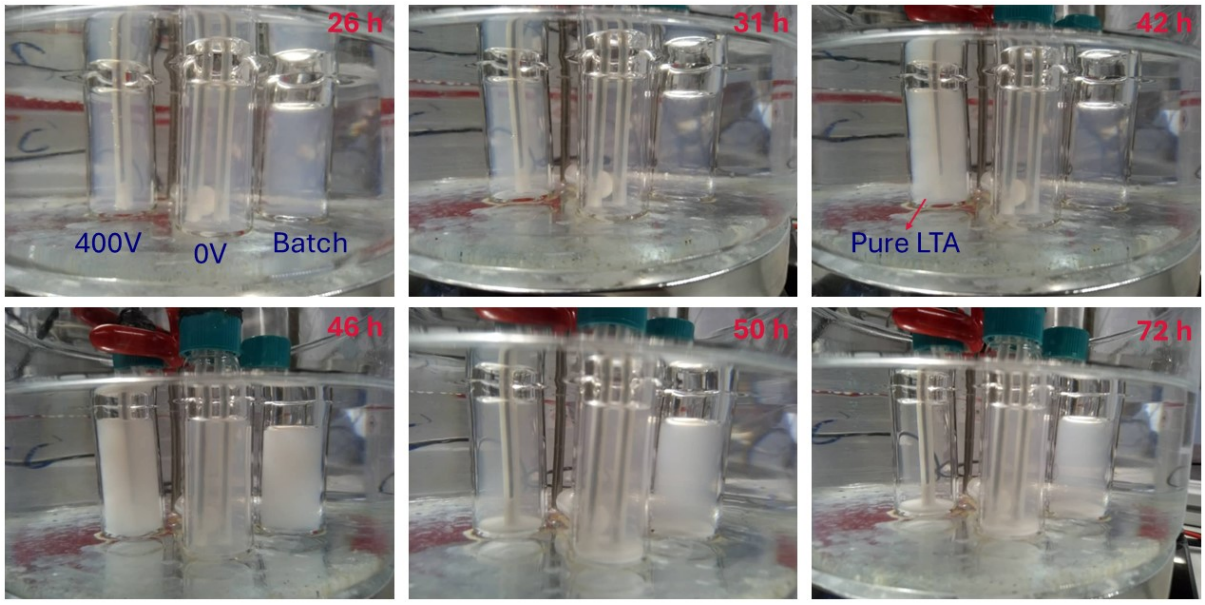

Figure S19. Photos of synthesis vials during the crystallization at different times for NaOH/Si of 0.04 in FAU/LTA system, Table S1, entry 2.

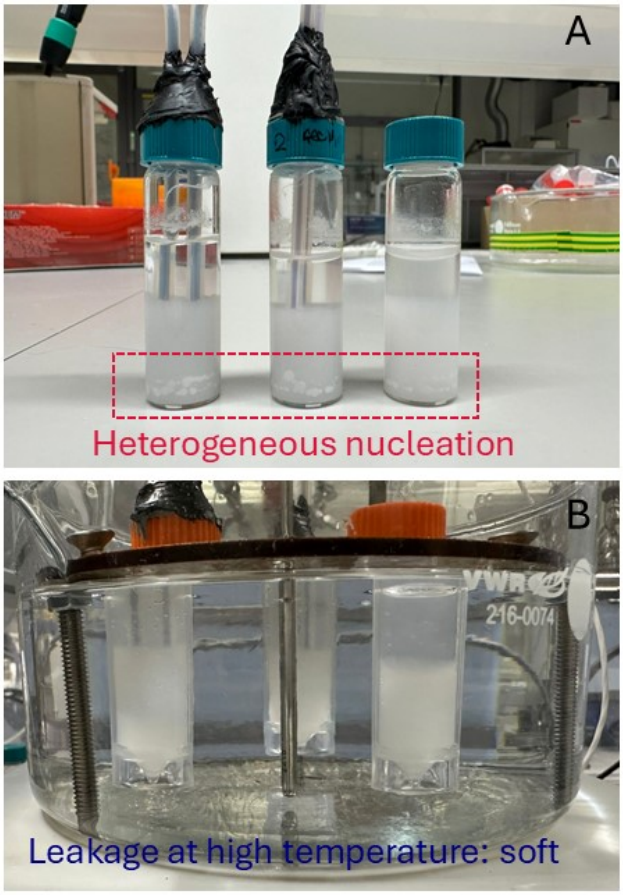

Figure S20. Low-silica CHA synthesis after 72 h at 100 ℃ A) inside the glass vials and B) inside polypropylene vials.

Extra experiments and results of FAU/LTA and trials for other systems under DC EFs using Type 2 reactors:

After initial successful experiments in the FAU/LTA system, subsequent results under 0 V and EKC conditions showed inconsistent trends (Figure S21). Initially, we suspected that the magnetic field generated by the stirring plate might be interfering with the applied EFs. To test this, we conducted experiments without stirring inside the heating oil, and later switched to a hot plate without a permanent magnetic stirrer. However, even under these adjusted conditions, the results remained diverse: phase selectivity did not consistently favor LTA under EKC, and occasionally shifted toward LTA even at 0 V_{PP} (Figure S21A and B). Further investigation revealed that the FAU/LTA system is susceptible to heterogeneous nucleation[13], particularly on the porous PTFE coating (Figure 2D, Type 2). This was evident when the 0 V synthesis showed a shift in phase selectivity toward LTA at low NaOH/Si ratios. Despite replacing the PTFE sheath around the Cu-wire with a new one, phase selectivity toward LTA under EF conditions was still not achieved repeatedly (Figure S21). Unfortunately, even in further investigation with other systems (in Type 2), including FAU/LTA without OSDA[5] and FAU/EMT[6], no clear influence of EKC on crystallization was observed (Figure S22A and B). With the Type 2 reactor, high-voltage, 3kV, trials were also performed. At 3kV, there was no clear effect of EKC on phase selectivity (Figure S23) and the aluminium content (Table S4) of a nano-sized NaA[7] zeolite, Na-UZM-9[8] (LTA framework) and BPH[9] at 60, 100 and 30 ℃, respectively.

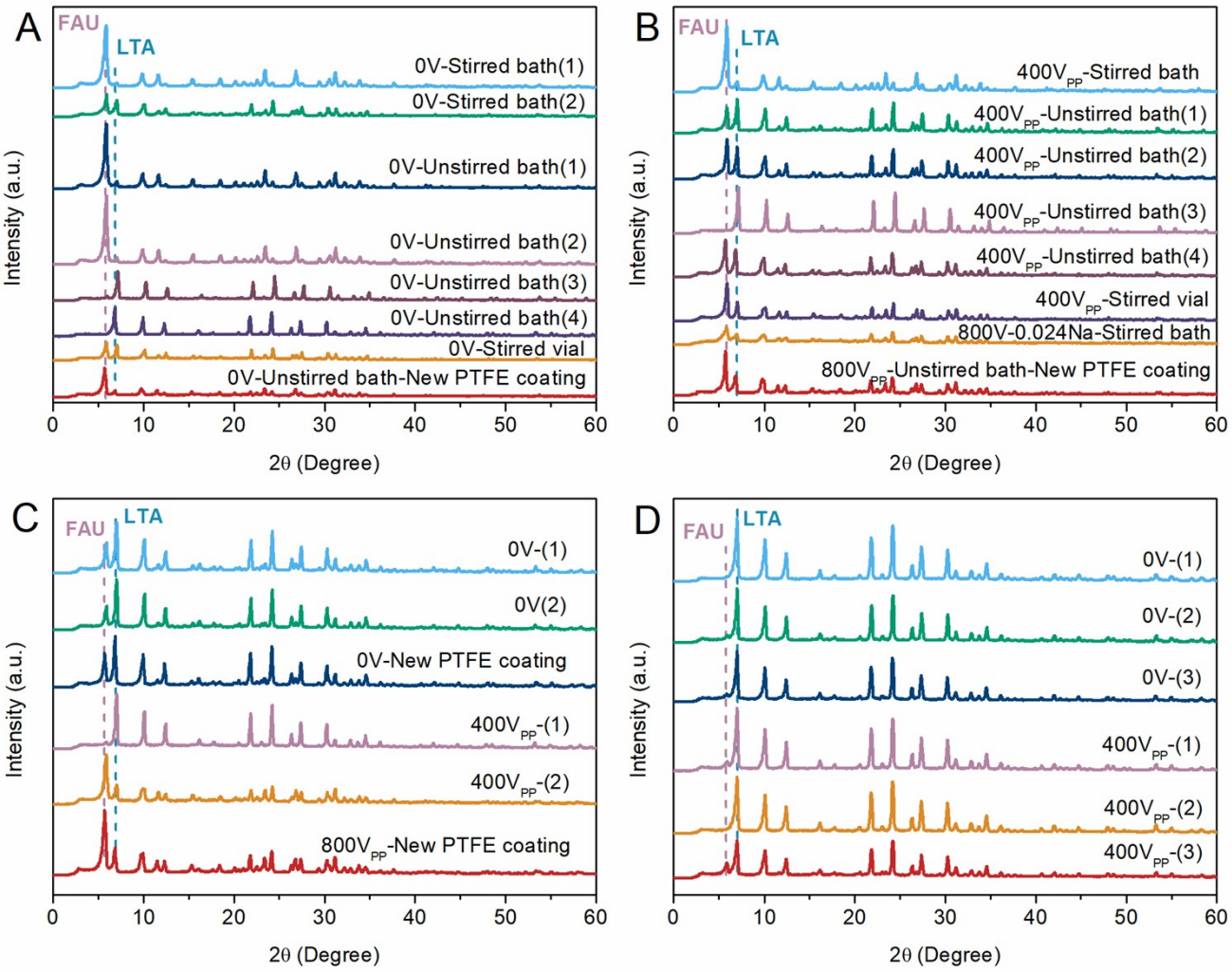

Figure S21. PXRD patterns of different trials for FAU/LTA synthesis at 0V and EKC conditions A&B) NaOH/Si ratio of 0.024, C) 0.032 and D) 0.04. For C and D, the oil bath was not stirred. FAU and LTA characteristic peaks are included as visual guides.

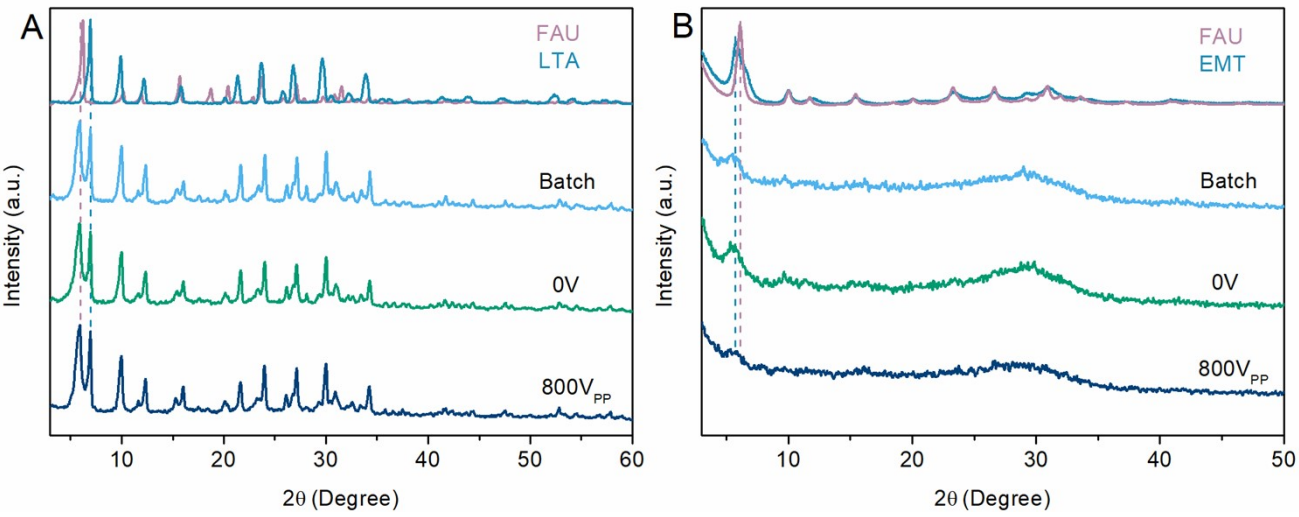

Figure S22. PXRD patterns of products obtained from synthesis of A) FAU/LTA system without OSDA. FAU and LTA reference patterns were measured from CBV300 and zeolite 4A. B) Nano-sized FAU/EMT zeolites. The reference patterns for nanosized FAU and EMT were collected from the IZA database. The synthesis compositions are presented in Table S1.

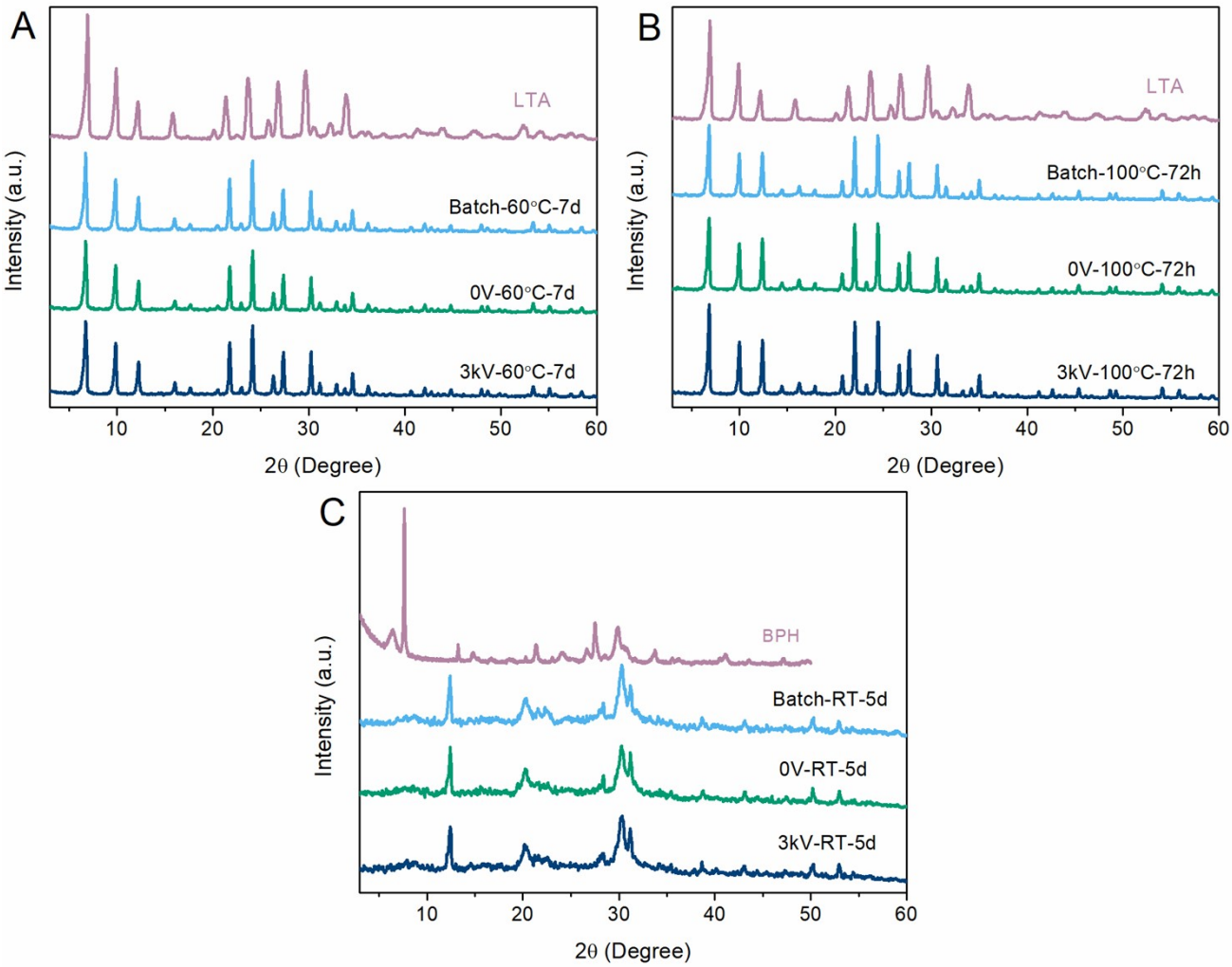

Figure S23. PXRD patterns of A) nano-sized NaA, B) Na-UZM-9 and C) BPH zeolites synthesized in 7 ml glass vials. The synthesis compositions are presented in Table S1. For C, the PXRD pattern does not match BPH structure according to the findings in the original work[9]. The LTA reference pattern was measured from Zeolite 4A and the BPH reference pattern was taken from the IZA database.

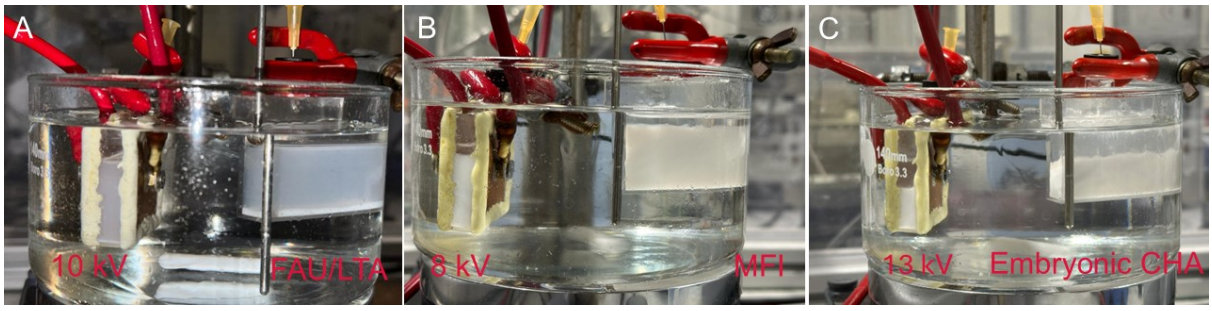

Figure S24. Photos of cuvette reactors during crystallization for different systems: A) FAU/LTA, B) MFI and C) Embryonic CHA.

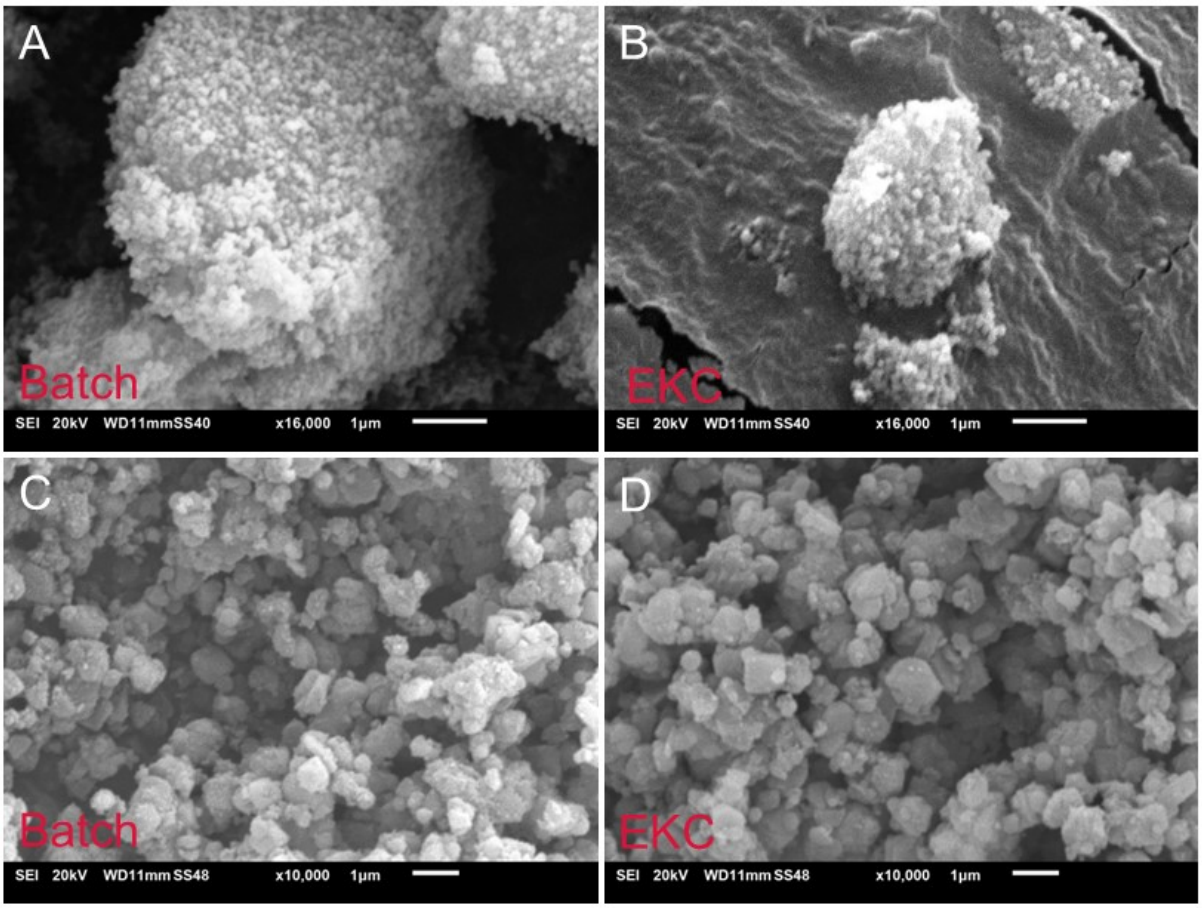

Figure S25. SEM images of products obtained from the synthesis of MFI zeolite in quartz cuvettes in A) batch and B) under **8 kV**, and embryonic CHA zeolite in C) batch and D) under **13 kV**.

Table S4. Si/Al ratio of zeolite samples. The elemental compositions were obtained from ICP-EOS analysis.

Sample	**Si/Al mol ratio**
7ml vials	
NaA-Batch	1.9
NaA-0V	1.9
NaA-3kV	1.9
Na-UZM-9-Batch	3.7
Na-UZM-9-0V	3.7
Na-UZM-9-3kV	3.7
Cuvette	
FAU/LTA-Batch	1.9
FAU/LTA-10kV	1.9
Embryonic CHA-Batch	12
Embryonic CHA-13kV	12

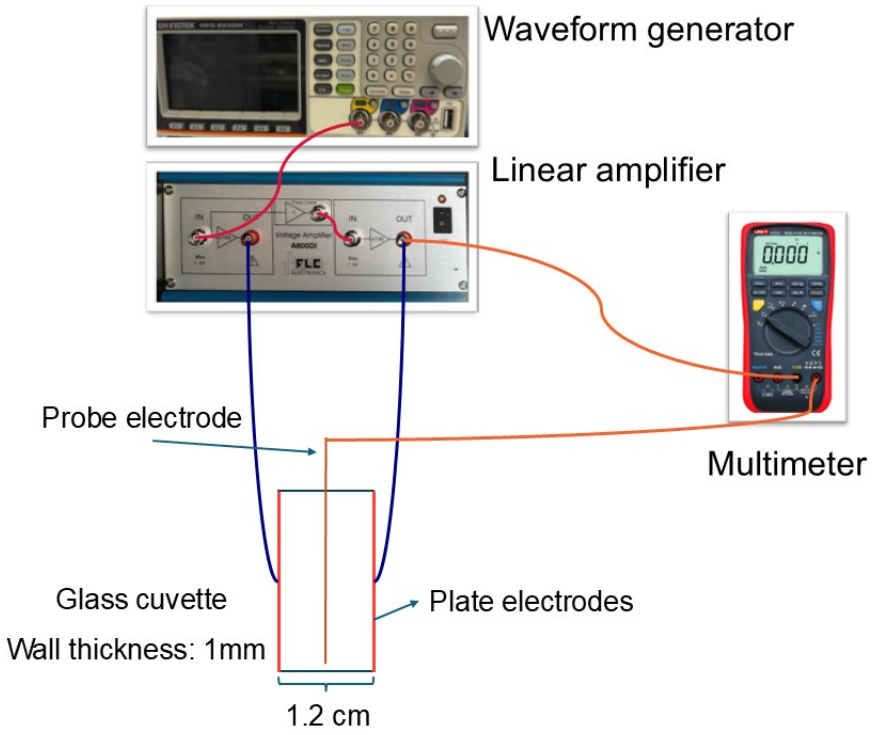

Figure S26. The setup's scheme for measuring the voltage inside the glass cuvette.

Electric double layer (EDL) calculation[14]**:**

$$\lambda^2 = \frac{\varepsilon_L KT}{e^2 I}$$

$$I = \sum_i m_i z_i^2$$

λ: *Deby length*

ε_L: *Electric permittivity of water*

I: *Ionic strength*

T: *Absolute temperature*

K: *Boltzmann constant*

m_i: *ion particles concentration*

z_i: *Valence of the ion*

e: *electronic unit charge*

For the mixture with the following composition:

$1\ Si{:}0.46\ Al{:}1.096\ TMA^+{:}0.024\ Na^+{:}1.120\ OH^-{:}56\ H_2O$

At temperature of 100 ℃, by considering Na as the only ion, the Debye length is 2.62 nm and by considering both Na and TMA, the Debye length decreases to 0.38 nm. These numbers show that the Debye-Hückel equation underestimates the Debye length at high ions concentration.

References

(1) Meier, W. M.; Groner, M. Zeolite Structure Type EAB: Crystal Structure and Mechanism for the Topotactic Transformation of the Na, TMA Form. *J. Solid State Chem.* **1981**, *37* (2), 204–218. https://doi.org/10.1016/0022-4596(81)90086-4.

(2) Fan, W.; Shirato, S.; Gao, F.; Ogura, M.; Okubo, T. Phase Selection of FAU and LTA Zeolites by Controlling Synthesis Parameters. *Microporous Mesoporous Mater.* **2006**, *89* (1–3), 227–234. https://doi.org/10.1016/j.micromeso.2005.11.001.

(3) Hasegawa, Y.; Abe, C.; Nishioka, M.; Sato, K.; Nagase, T.; Hanaoka, T. Influence of Synthesis Gel Composition on Morphology, Composition, and Dehydration Performance of CHA-Type Zeolite Membranes. *J. Memb. Sci.* **2010**, *363* (1–2), 256–264. https://doi.org/10.1016/j.memsci.2010.07.040.

(4) Liang, Y.; Jacobson, A. J.; Rimer, J. D. Strontium Ions Function as Both an Accelerant and Structure-Directing Agent of Chabazite Crystallization. *ACS Mater. Lett.* **2021**, *3* (2), 187–192. https://doi.org/10.1021/acsmaterialslett.0c00460.

(5) Maldonado, M.; Oleksiak, M. D.; Chinta, S.; Rimer, J. D. Controlling Crystal Polymorphism in Organic-Free Synthesis of Na-Zeolites. *J. Am. Chem. Soc.* **2013**, *135* (7), 2641–2652. https://doi.org/10.1021/ja3105939.

(6) Ng, E.-P.; Chateigner, D.; Bein, T.; Valtchev, V.; Mintova, S. Capturing Ultrasmall EMT Zeolite from Template-Free Systems. *Science.* **2012**, *335* (6064), 70–73. https://doi.org/10.1126/science.1214798.

(7) Huang, Y.; Li, M.; Shi, C.; Liu, Z.; Ren, B. Synthesis of Ultra-Small NaA Zeolite Nanocrystals at near Room Temperature. *J. Porous Mater.* **2023**, *30* (4), 1143–1147. https://doi.org/10.1007/s10934-022-01402-2.

(8) Park, M. B.; Ahn, S. H.; Nicholas, C. P.; Lewis, G. J.; Hong, S. B. Charge Density Mismatch Synthesis of Zeolite Beta in the Presence of Tetraethylammonium, Tetramethylammonium, and Sodium Ions: Influence of Tetraethylammonium Decomposition. *Microporous Mesoporous Mater.* **2017**, *240*, 159–168. https://doi.org/10.1016/j.micromeso.2016.11.013.

(9) Clatworthy, E. B.; Debost, M.; Barrier, N.; Gascoin, S.; Boullay, P.; Vicente, A.; Gilson, J.-P.; Dath, J.-P.; Nesterenko, N.; Mintova, S. Room-Temperature Synthesis of BPH Zeolite Nanosheets Free of Organic Template with Enhanced Stability for Gas Separations. *ACS Appl. Nano Mater.* **2021**, *4* (1), 24–28. https://doi.org/10.1021/acsanm.0c02925.

(10) Devos, J.; Robijns, S.; Van Goethem, C.; Khalil, I.; Dusselier, M. Interzeolite Conversion and the Role of Aluminum: Toward Generic Principles of Acid Site Genesis and Distributions in ZSM-5 and SSZ-13. *Chem. Mater.* **2021**, *33* (7), 2516–2531. https://doi.org/10.1021/acs.chemmater.0c04832.

(11) Yang, X.; Dib, E.; Lang, Q.; Guo, H.; Fu, G.; Wang, J.; Yi, Q.; Zhao, H.; Valtchev, V. Silicalite-1 Formation in Acidic Medium: Synthesis Conditions and Physicochemical Properties. *Microporous Mesoporous Mater.* **2022**, *329*, 111537. https://doi.org/10.1016/j.micromeso.2021.111537.

(12) *A800D - Pendulum Instruments*. https://pendulum-instruments.com/products/dual-channel-high-voltage-linear-amplifiers/a800d/ (accessed 2025-12-03).

(13) Oleksiak, M. D.; Soltis, J. A.; Conato, M. T.; Penn, R. L.; Rimer, J. D. Nucleation of FAU and LTA Zeolites from Heterogeneous Aluminosilicate Precursors. *Chem. Mater.* **2016**, *28* (14), 4906–4916. https://doi.org/10.1021/acs.chemmater.6b01000.

(14) Moreno, R. Colloidal Processing of Ceramics and Composites. *Adv. Appl. Ceram.* **2012**, *111* (5–

6), 246–253. https://doi.org/10.1179/1743676111Y.0000000075.